IRSA 2019

Session 3

Energy Efficiency and Electrical Drives

Optimal Energy Management Strategy Based on the Pontryagin's Minimum Principle for a Hybrid Train Powered by Fuel Cells and Batteries

Peng, Hujun[1], Rapol, Satish[1], Deng, Kai[1], Thul, Andreas[1], Löwenstein, Lars[3], Li, Weihan[2], Ünlübayir, Cem[2], Sauer, Dirk Uwe[2] and Hameyer, Kay[1]

[1]Institute of Electrical Machines (IEM)
[2]Electrochemical Energy Conversion and Storage Systems Group, Institute for Power Electronics and Electrical Drives (ISEA)
RWTH Aachen University, Germany
[3]Siemens Mobility GmbH, Vienna Austria

Abstract

An optimal energy management strategy for a fuel cell and lithium-ion battery hybrid train, based on the Pontryagin's Minimum Principle (PMP), is introduced in this paper. Particularly, the aging model of the battery is included for the sake of balancing the fuel economy and prolonging the lifetime of the battery in developing the energy management strategy. As the temperature strongly influences the aging effect, in this work, the lithiumion cells in the battery system are modeled considering the thermoelectric coupling effect. Due to the high dimensionality of the battery model, the energy management strategy based on the Pontryagin's Minimum Principle (PMP) is better suited to solve this problem class. By employing a strategy based on PMP, the estimation of the initial values of the so-called co-states remains crucial. Instead of using the classic shooting-method, a robust, and fast search mechanisms based on the differential evolution is developed, to find the proper initial co-states values.

Keywords: fuel cell hybrid train, optimal energy management strategy, Pontryagin's Minimum Principle, battery model, battery aging, differential evolution.

1 Introduction

The electrification of railway vehicles is an effective way to save energy and reduce emissions. However, the cost of complete electrification of the railway network, particularly for lines with low traffic, is not cost effective. For these railway sections, the fuel cell hybrid train is an efficient alternative. In a fuel cell hybrid train, a lithium-ion battery system is used in addition to fuel cells, providing and absorbing high transient power during acceleration and recuperative braking operation. Moreover, the hybrid train operates in charge-sustaining mode. Therefore, the fuel cell system meets the average power requirement and the battery system fulfills the transient peak power demand. The power distribution between the two energy storage systems, the energy management strategy (EMS), provides a degree of freedom to optimize the performance of the hybrid train, including the driveability, the hydrogen consumption and the fuel cell lifetime. Developing an energy management strategy under many constraints, defined globally or locally, is a challenging task. In the literature, there are basically three methods of developing energy management strategies: rule-based, local optimization based and global optimization based methods [2]. The rule-based method is based on the engineer's experience and implemented using conditional rules. Benefiting from the low computational effort, the rule-based strategy is real-time capable. However, it does not guarantee optimal performance [12]. The local optimization based method is also real-time capable because the power distribution is determined based on a predefined transient cost function. The most famous of them is the equivalent consumption minimization strategy (ECMS), which treats the battery power in a sense as fuel consumption in the future using an equivalent factor [16]. This method does not guarantee an optimal power distribution as well [2]. However, the optimal distribution is accessible if the drive cycle of the vehicle is known in advance, which is a reasonable assumption for railway transport. For this purpose, the global optimization based method is used. There are two subtypes under the global optimization based method: Dynamic Programming (DP) and Pontryagin's Minimum Principle (PMP) [11]. Both approaches require enormous computational time on conventional hardware setups. This is a reason to employ a simple battery model as can be found mainly in the literature [1, 17]. Under such a model simplification, the optimal energy management strategy problem has only one state variable: the SoC of the battery. The disadvantage of this model is that it is not sufficient to represent the real performance of the battery under high dynamic load profiles, which is strongly influenced by the thermal conditions. Besides, for developing the energy management strategy, in addition to minimizing the hydrogen consumption, a long life of the battery is aspired to reduce the overall cost. Therefore, the aging model should be included to consider the balance between the fuel economy and the battery lifetime. There are basically two types of aging models

for the battery: electrochemical models and empirical models [3]. Since the electrochemical models are not real-time available, the empirical models are used. In most literatures about battery aging, the battery temperature dynamic is modeled [18, 19, 22]. If the uneven temperature distribution within the battery pack is taken into account, several local temperatures need to be included as state variables in the system dynamics. However, DP cannot effectively solve problems with numerous variables due to the phenomenon of "Bellman's curse of dimensionality" [4]. Therefore, to determine the optimal strategy, strategies based on PMP are used [9, 10]. In developing strategies based on PMP, the biggest challenge is to estimate the initial values of the so-called co-states defined in the PMP. The number of co-states is identical to the number of the state variables. Under the numerous state variables, the classic shooting method and the deterministic methods are not numerically efficient to find the proper estimates of the co-states variables [13]. For this reason, in this paper, a robust, and fast search mechanisms based on the differential evolution is developed to find the proper estimates of the initial co-states variables. The paper is organized as follows: first, the hybrid train model and its subsystems are described; second, the basic principle of PMP and its application in EMS is introduced; third, the robust differential evolution algorithm is introduced; following, the results of optimum energy management strategy using PMP with the help of the differential evolution will be displayed. Based on that follows a investigation of the effect of a weighting factor between fuel economy and battery lifetime. Last, the conclusion and the possible outlook will be given.

2 Hybrid Train Driveline Model

The driveline configuration of the hybrid train is shown in Fig. 1. The fuel cell provides electric power through a DC-DC converter actively, and the battery passively supplies the residual power to fulfill the power demand. The sum of them is converted to the mechanical power in an electric motor, with the loss in inverter and motor deducted. Finally, the motor torque is transmitted through the gear and axle to the tire, which drives the train forward. The DC-DC converter is modeled using a constant efficiency of 0.98. For other subsystems, there are a detailed introduction in the following parts.

2.1 Longitudinal Dynamics

The drive cycle of the hybrid train is known as a priori knowledge to the energy management problem. Based on that, the corresponding road power can be determined using the inverse vehicle dynamic model. This demand power must be corrected because it might exceed the component capacity. For example, the traction power might be more than the power of both

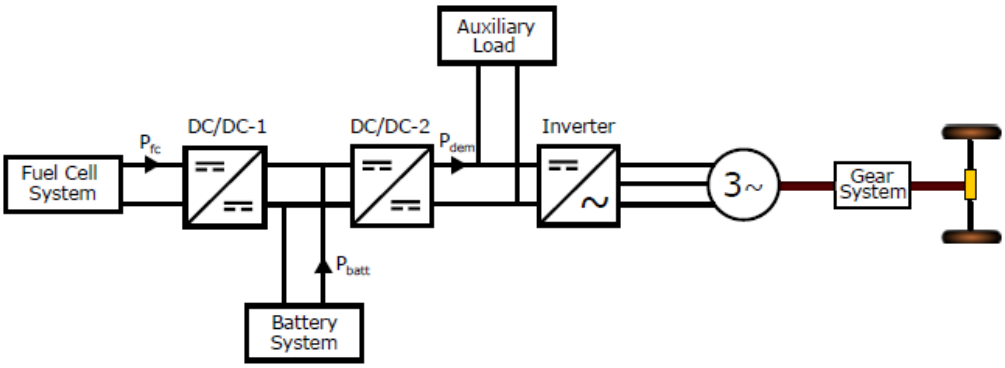

Figure 1: System configuration of hybrid train.

fuel cells and battery system, or the braking power may be out of the amount that can be collected by the battery system. This inverse dynamic model is based on the balance of forces. The force acting on the train consists of two parts: the traction force on the wheel and the various resistant force on the vehicle body. The difference between them accelerates or brakes the train. The various resistant forces on the vehicle body include aerodynamic drag, uphill resistance, and rolling resistance, that are generally depending on the vehicle velocity as shown in (1)

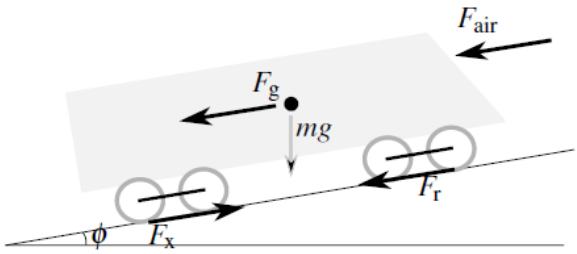

Figure 2: Forces acting on the train.

$$\begin{aligned} F_x &= F_a + F_r + F_{air} + F_g \\ &= \delta m\dot{v} + \mu_r mg\cos(\phi) + 0.5\rho_{air}C_d A_f v^2 + mg\sin(\phi), \end{aligned} \tag{1}$$

where m is the train mass; δ is the mass factor, combining the translational and rotational inertial together; μ_r is the coefficient of the rolling resistance; C_d is the aerodynamic coefficient; Af is the front area; g is gravitational acceleration and the ϕ is the angle of slope. Then, the power demand on the tire is

$$P_{req} = F_x v. \tag{2}$$

2.2 Axle and Transmission

For energy analysis, a lossy gear model is used, which takes into account power losses. Given that the speed ratio is equal to the gear ration g_{fb}, being given by kinematic constraints, where the subscripts b and f indicate the base and follower shaft. The power loss means a reduction of the torque at the output shaft, described using the gear efficiency η_{gear} as

$$T_{\mathrm{f}} = \begin{cases} \frac{\eta_{\mathrm{gear}}}{g_{\mathrm{fb}}} T_{\mathrm{b}} & \text{if } P_{\mathrm{b}} = T_{\mathrm{b}} \cdot \omega_{\mathrm{b}} \geq 0 \\ \frac{1}{\eta_{\mathrm{gear}} \cdot g_{\mathrm{fb}}} T_{\mathrm{b}}. & \text{if } P_{\mathrm{b}} = T_{\mathrm{b}} \cdot \omega_{\mathrm{b}} < 0 \end{cases}, \tag{3}$$

with the convention that power flow positive when going from b to f. The power loss is always positive and is computed as

$$P_{\mathrm{loss}} = \begin{cases} \omega_{\mathrm{b}} T_{\mathrm{b}} \left(1 - \eta_{\mathrm{gear}}\right) & \text{if } P_{\mathrm{b}} = T_{\mathrm{b}} \cdot \omega_{\mathrm{b}} \geq 0 \\ \omega_{\mathrm{f}} T_{\mathrm{f}} \left(1 - \eta_{\mathrm{gear}}\right) & \text{if } P_{\mathrm{b}} = T_{\mathrm{b}} \cdot \omega_{\mathrm{b}} < 0 \end{cases}. \tag{4}$$

The gear ratio is chosen to be 10 and the efficiency of the whole transmission and axle is considered to be at constant 0.98.

2.3 Electric Machine

The electrical motor is modeled using maps in function of torque and rotational speed, without considering dynamic. Desired torque and the actual rotational speed can be used as control inputs. There are four map used: power loss map P_{loss} (T_{em}; ω_{em}), current map I (T_{em}; ω_{em}), voltage map U (T_{em}; ω_{em}) and power factor map cosϕ (T_{em};ω_{em}). The relation between motor torque and electric power can be expressed as

$$P_{\mathrm{elec}} = T_{\mathrm{em}} \cdot \omega_{\mathrm{em}} + P_{\mathrm{loss}}\left(T_{\mathrm{em}}, \omega_{\mathrm{em}}\right). \tag{5}$$

When operating in motor mode, both the mechanic power $T_{\mathrm{em}} \bullet \omega_{\mathrm{em}}$ and the motor loss power P_{loss} (T_{em}; ω_{em}) are positive, then the input electric power P_{elec} is the sum of them; when operating in generator mode, the mechanic power $T_{\mathrm{em}} \bullet \omega_{\mathrm{em}}$ is negative and the motor loss power P_{loss} (T_{em}; ω_{em}) is still positive, then the output electric power P_{elec} is the difference of them. Except the power loss map, the other three maps are also used to analytically calculate the power loss in the inverter, which will be introduced in the next part.

2.4 Inverter

The two level inverter provides sinusoidal currents and voltages. As a result, the duty cycle and the motor current change in each switching pulse. To calculate the average power loss during a electrical period, the loss must be calculated for each switching cycle and be added up. Since this procedure is very complex, an alternative, simple calculation method is used. By assuming sinusoidal quantities, an analytical calculation of the switching losses with the parameters of the circuit breaker is possible. The derivation of the equations can be taken from the work of Mestha [15] and Casanelas [5]. Instead of giving the detailed deriving process, the resulting formulas are listed in equation (6)) – (7)

$$P_{\text{C-IGBT}} = \frac{u_{\text{CE-0}} \cdot \hat{i}}{2\pi} \cdot \left(1 + \frac{\hat{a} \cdot \pi}{4} \cdot \cos\phi\right) + \frac{r_{\text{CE}} \cdot \hat{i}^2}{2\pi} \cdot \left(\frac{\pi}{4} + \hat{a}\left(\frac{2}{3} \cdot \cos\phi\right)\right), \tag{6}$$

$$P_{\text{C-diode}} = \frac{u_{\text{F-0}} \cdot \hat{i}}{2\pi} \cdot \left(1 - \frac{\hat{a} \cdot \pi}{4} \cdot \cos\phi\right) + \frac{r_{\text{F}} \cdot \hat{i}^2}{2\pi} \cdot \left(\frac{\pi}{4} - \hat{a}\left(\frac{2}{3} \cdot \cos\phi\right)\right). \tag{7}$$

The conduction loss in IGBT $P_{\text{C-IGBT}}$ and diode $P_{\text{C-Diode}}$ depends on the motor current $\hat{i}$, the degree of modulation $\hat{a}$, the power factor $cos\phi$ and the component parameters. For the switching loss follows

$$P_{\text{S-IGBT}} = \frac{1}{\pi} \cdot f_s \cdot (E_{\text{on}} + E_{\text{off}}) \cdot \frac{U_{\text{dl}}}{U_{\text{ref}}} \cdot \frac{i}{I_{\text{ref}}}, \tag{8}$$

$$P_{\text{S-diode}} = \frac{1}{\pi} \cdot f_s \cdot (E_{\text{REC}}) \cdot \frac{U_{\text{dl}}}{U_{\text{ref}}} \cdot \frac{\hat{i}}{I_{\text{ref}}}, \tag{9}$$

where fs is the switching frequency; E_{on} and E_{off} are switching-on loss and switching-of loss of IGBT respectively; E_{REC} the switching-off loss of Diode; U_{dl} the dc-link voltage; U_{ref} and I_{ref} the reference voltage and current corresponding to the E_{on}, E_{off} and E_{REC}.

The total loss of the inverter are composed of all individual losses multiplied by the number of inverter legs

$$P_{\text{loss-total}} = 6 \cdot (P_{\text{C-IGBT}} + P_{\text{C-diode}} + P_{\text{S-IGBT}} + P_{\text{S-diode}}). \tag{10}$$

3 Lithium Ion Battery System

Here, a high-power LiNi-CoMnO2 cathode and graphite-based anode cell is considered. To achieve a balance between the model accuracy and computation burden of energy management, a zeroth order equivalent circuit model (ECM) is implemented to model the lithium-ion battery dynamics. As mentioned prior, to capture the thermoelectric effect,

the temperature dynamics of the battery is also well thought-out here. The zeroth order is expressed in equation (11) [20]

$$U_{\text{t-cell}} = U_{\text{ocv-cell}}(SOC, \theta) - I_{\text{cell}} \cdot R_{\text{0-cell}}(SOC, \theta), \tag{11}$$

where $U_{\text{t-cell}}$ represents the cell terminal voltage, $U_{\text{ocv-cell}}$ represents the open-circuit voltage of the cell which is a function of both, the temperature q and SOC of the cell, $R_{\text{0-cell}}$ represents the cell resistance which is again a function of both, the temperature q and SOC of cell and I_{cell} represents the current produced by the cell. Battery SOC which is one of the dynamics in the optimal control problem ahead is calculated by the total amount of charge stored in the cell, relative to the nominal charge capacity of the cell, which is given by equation (12) [20]

$$SOC = SOC_0 - \frac{1}{Q_{\text{cell}}} \int_{t_0}^{t} I_{\text{cell}}(t)dt. \tag{12}$$

Battery Pack Configuration: Herein, in total 250 cells are connected in series and 100 cells are connected in parallel, resulting in a battery Battery pack power is given by equation (13)

$$P_{\text{batt}} = U_{\text{ocv-batt}} \cdot I_{\text{batt}} - {I_{\text{batt}}}^2 \cdot R_{\text{0-batt}}. \tag{13}$$

And the battery current evaluated by equation (14)

$$I_{\text{batt}} = \frac{U_{\text{ocv-batt}}}{2 \cdot R_{\text{0-batt}}} - \sqrt{\left(\frac{U_{\text{ocv-batt}}}{2 \cdot R_{\text{0-batt}}}\right)^2 - \frac{P_{\text{batt}}}{R_{\text{0-batt}}}}. \tag{14}$$

Here for simplicity, the dc-dc converter between the battery pack and the dc-link is assumed to work with constant efficiency.

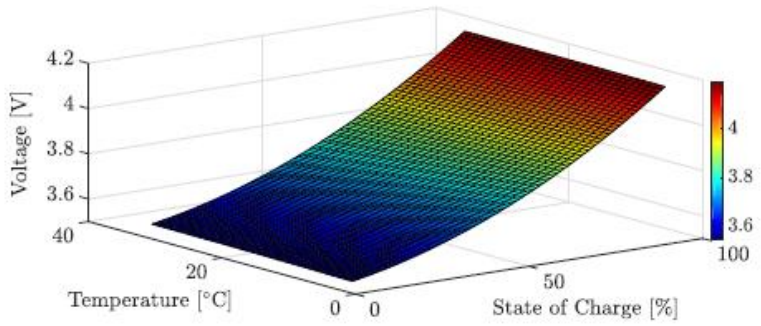

Figure 3: Characteristics of the open-circuit voltage of the lithium-ion cell.

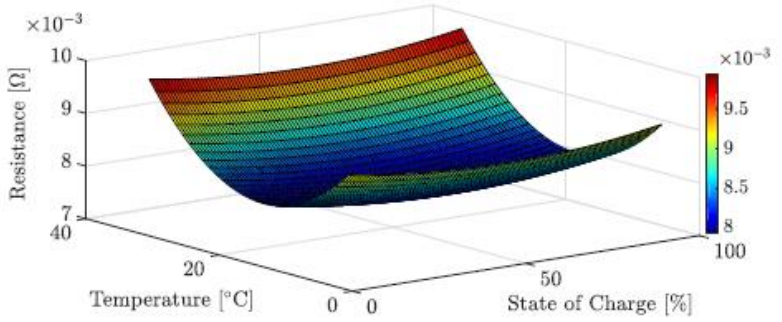

Figure 4: Characteristics of the resistance of the lithium-ion cell.

The battery aging is considered by taking into account the capacity degradation model, which is given by equation (15) [23]

$$Q_{\text{loss}\%} = (\alpha \cdot SOC + \beta) \cdot \exp\left(\frac{-31700 + 163.3 \cdot I_{\text{c-nom}}}{R \cdot \theta}\right) \cdot Ah^{0.57}, \tag{15}$$

With

$$\alpha = \begin{cases} 1287.6, & SOC \leqslant 0.45 \\ 1385.5, & SOC > 0.45 \end{cases} \quad \beta = \begin{cases} 6356.3, & SOC \leqslant 0.45 \\ 4193.2, & SOC > 0.45 \end{cases},$$

and θ is the cell temperature in Kelvin, $I_{\text{c-norm}}$ the nominal C-rate, *Ah* the total charge throughput from the cell and *R* the gas constant. Battery end of life is defined as 20% loss of capacity and the battery life at the nominal current rate of 1C, nominal temperature and nominal SOC is determined by equation (16) [14]

$$\Gamma = \left[\frac{20}{(\alpha \cdot SOC_{\text{nom}} + \beta) \cdot \exp\left(\frac{-31700 + 163.3 \cdot I_{\text{c-nom}}}{R \cdot \theta_{\text{nom}}}\right)}\right]^{\frac{1}{0.57}}. \tag{16}$$

Whereas the actual battery life calculated at the actual current rate, temperature and SOC is determined by equation (17) [14]

$$\gamma(SOC, I_c, \theta_{\text{batt}}) = \left[\frac{20}{(\alpha \cdot SOC + \beta) \cdot \exp\left(\frac{-31700 + 163.3 \cdot I_c}{R \cdot \theta_{\text{batt}}}\right)}\right]^{\frac{1}{0.57}}. \tag{17}$$

The relative ageing effect is calculated by the severity factor s and is evaluated as per equation (18) [21]

$$\sigma\left(I_c, \theta_{batt}, SOC\right) = \frac{\Gamma}{\gamma(I_c, \theta_{batt}, SOC)}. \tag{18}$$

Consequently, the effective Ah throughput from the battery after considering the relative severity affect s is calculated by equation (19) [23] [21]

$$Ah_{eff}(t) = \int_0^t \sigma\left(I_c, \theta_{batt}, SOC\right) \cdot |I(t)| dt. \tag{19}$$

3.1 Fuel Cell

There are various types of fuel cells which are categorized in terms of their electrolyte. In this work, the Polymer-Electrolyte- Proton Exchange Membrane (PEM) is used. Accurately modeling the total fuel cell system related to multiple disciplines is complicated. Therefore, it is common to use a quasi-static model of the fuel cell in energy management application. Without considering the complex thermodynamic and electrochemistry equations, a model based on an efficiency map in Fig. 5 is used. According to this map, the hydrogen consumption rate can be calculated as

$$\dot{m}_{H_2} = \frac{P_{fc}}{\eta\left(P_{fc}\right) \times Q_{LHV}}, \tag{20}$$

where P_{fc} is the net power output of the fuel cell; Q_{LHV} is the lower heating value of hydrogen and η (P_{fc}) the efficiency of the total fuel cell system corresponding

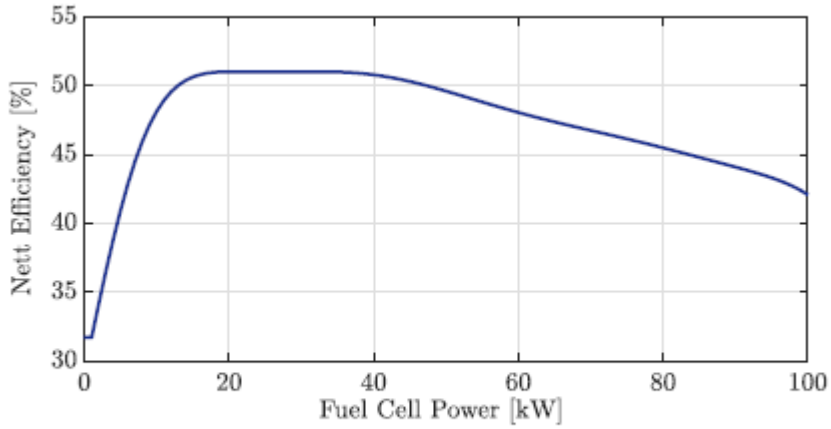

Figure 5: Characteristics of fuel cell net efficiency.

4 Pontryagin's Minimum Principle

Pontryagin's Minimum Principle (PMP) is a very computationally efficient optimal control method to find the global optimum of an objective function. Unlike Dynamic Programming, PMP method is efficient for higher dimension problems too. In this method, the optimal control value is achieved by considering state dynamic constraints and the boundary conditions of the state variables. This is accomplished by minimising the Hamiltonian for all the feasible values in control domain at each time instant, which is given by equation (21)

$$u^*(t) = \arg\min_{u(t)}(H(x(t),u(t),\lambda(t),t)). \tag{21}$$

Where Hamiltonian is defined by equation (22)

$$H(x(t),u(t),\lambda(t),t) = L(x(t),u(t),t) + \lambda(t)\cdot f(x(t),u(t),t), \tag{22}$$

where *L(x(t);u(t); t*) is the integrand of an objective function *J* to be minimized, which is defined like following

$$J = \int_0^t L(x(t),u(t),t)dt, \tag{23}$$

and *f (x(t);u(t); t)* is a vector of the state dynamics.

$x(t)$: state variables vector, lower limit $\leq x \leq$ upper limit
$u(t)$: control variable vector, lower limit $\leq u \leq$ upper limit
$\lambda(t)$: co-state vector.

The dynamics of the states and co-states are determined by equation (24) and (25) respectively

$$\dot{x}(t) = \frac{\partial}{\partial\lambda}H(x(t),u(t),\lambda(t),t), \tag{24}$$

$$\dot{\lambda}(t) = -\frac{\partial}{\partial x}H(x(t),u(t),\lambda(t),t). \tag{25}$$

4.1 Problem formulation for EMS in a hybrid vehicle

In this configuration, the fuel cell power is the primary active source of energy, and the battery power is to support the transient demands in the Hybrid vehicle. The EMS objective here is to use this one degree of freedom between two sources and thereby determine the optimal load share between the two sources of power and consequently minimise the H_2 fuel consumed. Additionally, the EMS also targets towards prolonging the battery life.

To achieve the abovestated objectives, we define both the control variable $u = P_{fc}$ and power demand as P_{dem} in kW, where demand power is depending upon the vehicle's drive cycle. Here, a cost function which considers the economical fuel consumption and battery ageing simultaneously is derived. The fuel consumption minimisation is given by equation (26)

$$J_1 = \int_{t_0}^{t_f} \dot{m}_{fc}\,(u(t), P_{dem}(t))\,dt. \tag{26}$$

Where $\dot{m}_{fc}$ is the H_2 mass flow rate in grams per sec which is given by equation (27)

$$\dot{m}_{fc} = 2.531 \cdot e^{-5} \cdot u^2(t) + 0.01615 \cdot u(t). \tag{27}$$

Battery ageing minimization is considered by minimizing the effective Ah throughput which is given by equation (28)

$$J_2 = \int_{t_0}^{t_f} \sigma \cdot |I_{batt}(t)|\,dt. \tag{28}$$

Consequently the two objectives as defined in equation (26) and (28) are combined together with varying weighting factor α ranging from 0 to 1. Here normalization of the individual costs is done by dividing with the corresponding maximum values. Therefore the resulting normalized cost function to be minimized is given by equation (29)

$$J = \int_{t_0}^{t_f} \left(\alpha \cdot \frac{\dot{m}_{fc}(t)}{\dot{m}_{fc-max}} + (1-\alpha) \cdot \frac{\sigma \cdot |I_{batt}(t)|}{|I_{batt\text{-}max}|} \right) dt, \tag{29}$$

where $\dot{m}_{fc\text{-}max}$ and $|I_{batt\text{-}max}|$ are the bases to normalize the cost function. The system states considered in this case are the state of charge and the temperature of the battery pack, and its dynamics are given by equation (30) and (31),

$$\dot{x}_1(t) = -\frac{U_{ocv-batt}\,(x_1,x_2) - \sqrt{U^2_{ocv-batt}\,(x_1,x_2) - 4 \cdot P_{batt}\,(P_{dem}(t), u(t))}}{2 \cdot Q_{batt} \cdot R_{0-batt}\,(x_1,x_2)}, \tag{30}$$

$$\dot{x}_2(t) = \frac{\dot{q}_{batt} + h_{batt} \cdot A_{surf} \cdot (\theta_{cool} - x_2(t))}{M_{batt} \cdot C_{p-batt}}, \tag{31}$$

where,

A_{surf}	:	Battery pack surface area	Q_{batt}	:	Battery charge capacity
M_{batt}	:	Battery pack mass	q_{batt}	:	Heat loss
$C_{p\text{-}batt}$	:	Specific heat capacity	h_{batt}	:	Heat transfer coefficient
θ_{cool}	:	Ambient temperature			

The corresponding Hamiltonian with the cost function coupled with the two system state dynamics is given by equation (32)

$$H = \alpha \cdot \frac{\dot{m}_{\mathrm{fc}}}{\dot{m}_{\mathrm{fc-max}}} + \frac{(1-\alpha)\cdot\sigma\cdot|I_{\mathrm{batt}}(t)|}{|I_{\mathrm{batt-max}}|} - \lambda_1 \cdot \frac{U_{\mathrm{ocv-batt}}(x_1,x_2) - \sqrt{U^2_{\mathrm{ocv-batt}}(x_1,x_2) - 4\cdot P_{\mathrm{batt}}(P_{\mathrm{dem}}(t),u(t))}}{2\cdot Q_{\mathrm{batt}}\cdot R_{0-\mathrm{batt}}(x_1,x_2)} + \lambda_2 \cdot \frac{\dot{q}_{\mathrm{batt}} + h_{\mathrm{batt}}\cdot A_{\mathrm{surf}}\cdot(\theta_{\mathrm{cool}} - x_2(t))}{M_{\mathrm{batt}}\cdot C_{\mathrm{p-batt}}}. \quad (32)$$

The dynamics of the co-states are calculated by equation (33) and (34)

$$\dot{\lambda}_1(t) = -\frac{1-\alpha}{|I_{\mathrm{batt-max}}|}\cdot\left(\frac{\partial\sigma}{\partial x_1}\cdot|I_{\mathrm{batt}}(t)| + \sigma\cdot\frac{\partial|I_{\mathrm{batt}}(t)|}{\partial x_1}\right) - \lambda_1(t)\cdot\frac{\partial\dot{x}_1}{\partial x_1} - \frac{\lambda_2(t)}{M_{\mathrm{batt}}\cdot C_{\mathrm{p-batt}}}\cdot\left(2I_{\mathrm{batt}}(t)\cdot R_{0-\mathrm{batt}}\frac{\partial I_{\mathrm{batt}}(t)}{\partial x_1} + I^2_{\mathrm{batt}}(t)\cdot\frac{\partial R_{0-\mathrm{batt}}}{\partial x_1}\right), \quad (33)$$

$$\dot{\lambda}_2(t) = -\frac{1-\alpha}{|I_{\mathrm{batt-max}}|}\cdot\left(\frac{\partial\sigma}{\partial x_2}\cdot|I_{\mathrm{batt}}(t)| + \sigma\cdot\frac{\partial|I_{\mathrm{batt}}(t)|}{\partial x_2}\right) - \lambda_1(t)\cdot\frac{\partial\dot{x}_1}{\partial x_2} - \frac{\lambda_2(t)}{M_{\mathrm{batt}}\cdot C_{\mathrm{p-batt}}}\cdot\left(2I_{\mathrm{batt}}(t)\cdot R_{0-\mathrm{batt}}\frac{\partial I_{\mathrm{batt}}(t)}{\partial x_2} + I^2_{\mathrm{batt}}(t)\cdot\frac{\partial R_{0-\mathrm{batt}}}{\partial x_2} - h_{\mathrm{batt}}\cdot A_{\mathrm{surf}}\right). \quad (34)$$

In using PMP as the optimal control strategy, the most critical part is choosing the right initial co-states values. It is critical as only the correct initial values of co-states can satisfy the requirements of the problem statements. One of them being end SOC equal to the initial SOC and the end value of co-state λ_2 equal to zero. λ_2 end value equal to zero is the requirement of an optimal condition in PMP, in this case as unlike the case of SoC, the end value of the second state variable, i.e. the temperature is not fixed. Further, an efficient way to find the correct co-states is explained in section 5.

5 Differential Evolution

Instead of shooting method, the evolutionary algorithm will be used to find proper estimates of the initial co-states values. The evolutionary algorithm is suitable for the high-dimensional multi-constrained optimization problem, which mathematically written as

$$\begin{cases} \min[f_1(\boldsymbol{x}), f_2(\boldsymbol{x}), \ldots, f_k(\boldsymbol{x})] \\ \text{subject to} \quad g_i(\boldsymbol{x}) \le 0, \text{with}\,(i = 1,2,\ldots,m) \end{cases}. \quad (35)$$

The $\boldsymbol{x} = [x_1, x_2, \ldots, x_D]$ is a vector of design variables with the dimension D. The k is the number of objectives and $k = 1$ and $k > 2$ stand for single-objective and multi-objective

optimization problems respectively. The m is the number of constrains in form of inequality. All the evolutionary algorithms share the following common process: crossover, mutation and selection, as displayed in Fig. 6. They differ from each other in the fourth step, how the new solutions are created from the old solutions. The most representative and the easiest to tun of these is the differential evolution (DE). In the following, the principle and the mechanism for adapting and improving the algorithm are presented in detail.

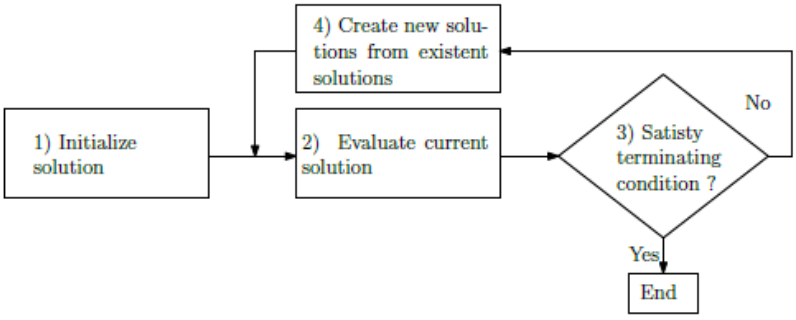

Figure 6: General outline of evolutionary algorithm.

5.1 Principle of Differential Evolution

The following matrix saves the population with N individuals in the g-th generation. Each row of the matrix $\boldsymbol{x}_i^g = \left(x_{i,1}^g\ x_{i,2}^g\ x_{i,3}^g\ \ldots\ x_{i,D}^g\right)$ represents a solution vector with the dimension of *D*.

$$\boldsymbol{X}^{\mathrm{g}} = \begin{pmatrix} x_{1,1}^g & x_{1,2}^g & x_{1,3}^g & \cdots & x_{1,D}^g \\ x_{2,1}^g & x_{2,2}^g & x_{2,3}^g & \cdots & x_{2,D}^g \\ \vdots & \vdots & \vdots & \ddots & \vdots \\ x_{N,1}^g & x_{N,2}^g & x_{N,3}^g & \cdots & x_{N,D}^g \end{pmatrix}. \tag{36}$$

For mutation, a donor vector corresponding to each target vector is generated using difference formulation from the randomly selected members of the current population as follows

$$\boldsymbol{v}_i^g = \boldsymbol{x}_{r3}^g + F_\alpha \cdot \left(\boldsymbol{x}_{\mathrm{best}}^g - \boldsymbol{x}_{r2}^g\right) + F_\beta \cdot \left(\boldsymbol{x}_i^g - \boldsymbol{x}_{r1}^g\right), \tag{37}$$

where $\boldsymbol{x}_{r1}^g$, $\boldsymbol{x}_{r2}^g$, $\boldsymbol{x}_{r3}^g$ are randomly selected, different individuals from the population in the gth generation without the target vector $\boldsymbol{x}_i^g$ included to create the donor vector $\boldsymbol{v}_i^g$. The vector $\boldsymbol{x}_{best}^g$ is the best individual of the population in terms of the objective value. The factors F_α and F_β are scaling factors. Moreover, there are other difference formulation

strategies, which can be found in [6]. The difference formulation here utilizes the information of the best solution to accelerate the convergence process. After the mutation, crossover between the donor vector and the target vector is implemented to create a trial using the binary recombination like

$$u_{i,j}^{g} = \begin{cases} v_{i,j}^{g} & \text{if} \quad rand_j(0,1) \le CR \quad \text{or} \quad j = j_{\text{rand}} \\ x_{i,j}^{g} & \text{otherwise} \end{cases}. \tag{38}$$

Where $rand_j$ (0;1) is a random number between 0 and 1 for the j-th dimension of each trial vector, to be compared with the control parameter CR, which describes how likely a dimension of the new trial vector comes from the donor vector. In contrast, the (1 – CR) means with which probability, a dimension comes from the target vector. The number j_{rand} is a random integer from the set {1,2,…,*D*} to ensure that at least one dimension comes from the donor vector such that the trial vector $\boldsymbol{u}_i^g$ differs from the target vector $\boldsymbol{x}_i^g$ by at least one dimension. Finally, the trial vector $\boldsymbol{u}_i^g$ will be compared with the target vector $\boldsymbol{x}_i^g$ and the winner go into the next generation.

5.2 Constraints handling

As mentioned, the critical point in using PMP is to find the optimal initial values of the costates $\lambda_{1\text{-t0}}$ and $\lambda_{2\text{-t0}}$, that satisfies the following boundary conditions

$$\lambda_{2\text{-tf}} = 0, \tag{39}$$

$$SOC_{\text{tf}} = SOC_{\text{t0}}. \tag{40}$$

The problems with equality in the constraint are difficult to solve using differential evolution. Therefore, the boundary condition is relaxed into the form that is appropriate to differential evolution, with the absolute end value of the second co-state $|\lambda_{2\text{-tf}}|$ as the goal function to minimize and the SOC_{tf} included in an inequality equation with tolerance

$$|SOC_{\text{t0}} - SOC_{\text{tf}}| \le 10^{-7}. \tag{41}$$

To incorporate the constraints violation degree into the definition of fitness function, the penalty function is often applied [8]. The penalty should be low at the beginning of the optimization, to benefit exploration, and increased with the evolution, to ensure that all the solutions at the end of optimization comply with the constraints. It's difficult to define such a dynamic penalty function, so another way is chosen. The fitness function is differently defined dependent on that, whether the solution feasible is or not as follows

$$f(\boldsymbol{x}) = \begin{cases} f(\boldsymbol{x}) & \text{if } \boldsymbol{x} \text{ is feasible} \\ \sum g_j & \text{otherwise} \end{cases}. \tag{42}$$

If the solution is feasible, the fitness value is directly equal to the objective, otherwise, the overall constraints violation degree will be signed to the fitness value. Based on that, there are three cases when comparing two solutions [7]:

1. If both solutions are valid, the solution with better objective function value will win,
2. If one solution is valid and the other solution is invalid, the valid solution will prevail,
3. If both solutions are invalid, the solution with less injury will win.

6 Simulation Results

The results discussed here are obtained by implementing the offline optimal control strategy PMP.

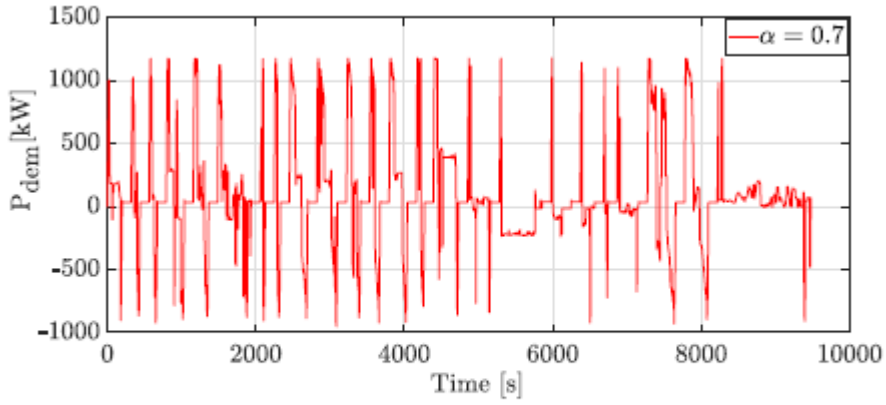

Figure 7: Power demand flow.

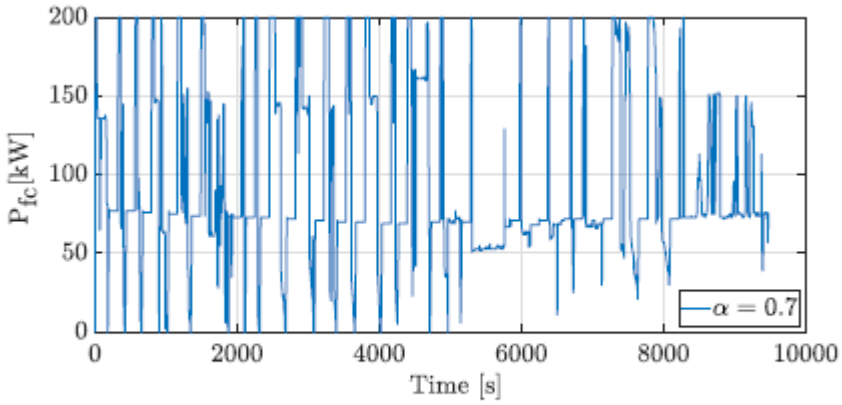

Figure 8: Fuel cell power flow.

Battery SOC: Figure 9 shows the battery state of charge profile. It can be seen that as the weighting factor "1 – α" associated with the cost function J_2 increases in magnitude in equation (29), the battery usage is decreased. In all the cases, the battery SOC_{t0} at the beginning of the drive cycle is equal to the SOC_{tf} at the end of the drive cycle. Thus, the boundary condition is satisfied by the optimal initial co-states values.

Co-state λ_1: Figure 10 details the evolution of the co-state λ_1 over the entire drive cycle. It can be observed that the absolute value of the co-state largely remains almost constant over

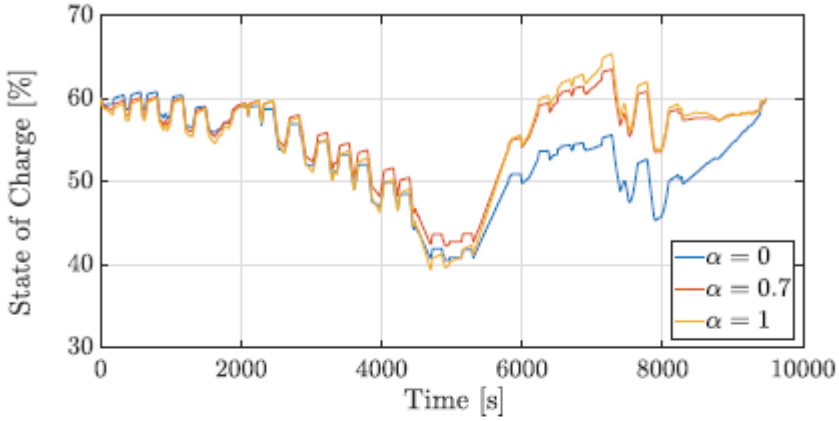

Figure 9: State of Charge.

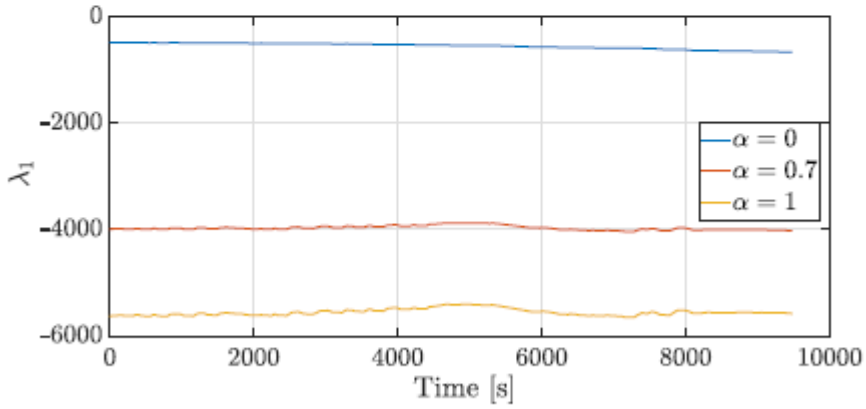

Figure 10: Co-state: λ_1.

the entire duration.

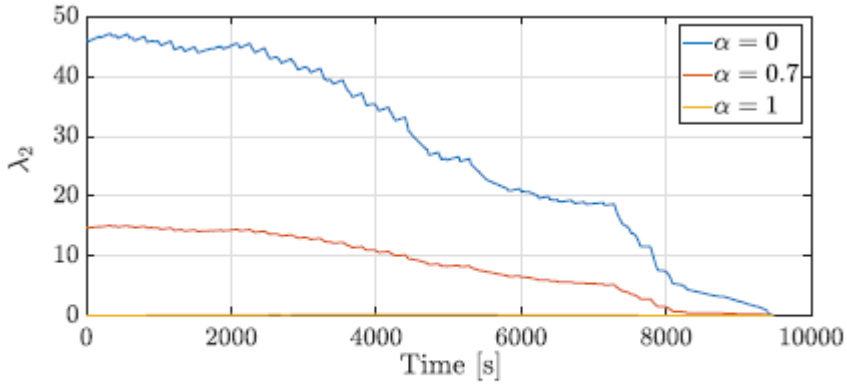

Figure 11: Co-state: λ_2.

Co-state λ_2: Figure 11 details the evolution of the co-state λ_2 over the entire drive cycle. Unlike co-state λ_1, which has no requirement of a fixed end state value, here the co-state λ_2 associated with the battery temperature must have an end value of zero.

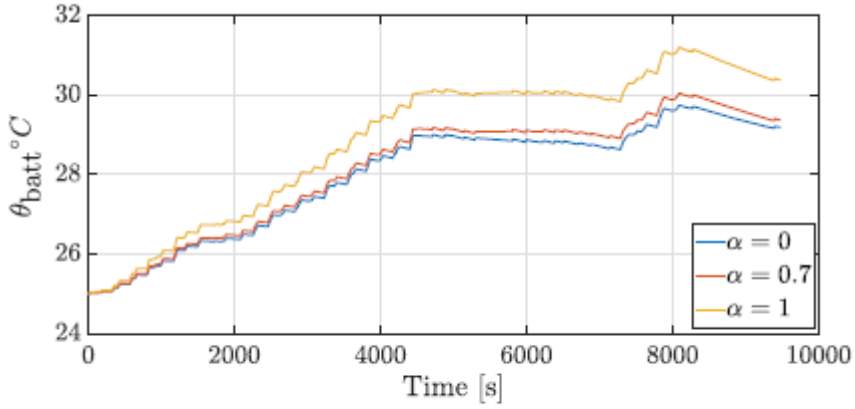

Figure 12: Battery Pack Temperature.

Battery pack Temperature θ_{batt}: Figure 12 details the evolution of the battery pack temperature θ_{batt} over the entire drive cycle. Here it can be observed that with the increasing "1 – α " factor on the cost J_2 in equation (29), the battery pack maximum temperature is decreased. This decrease is obviously due to the reduction in the total Ah throughput of the battery.

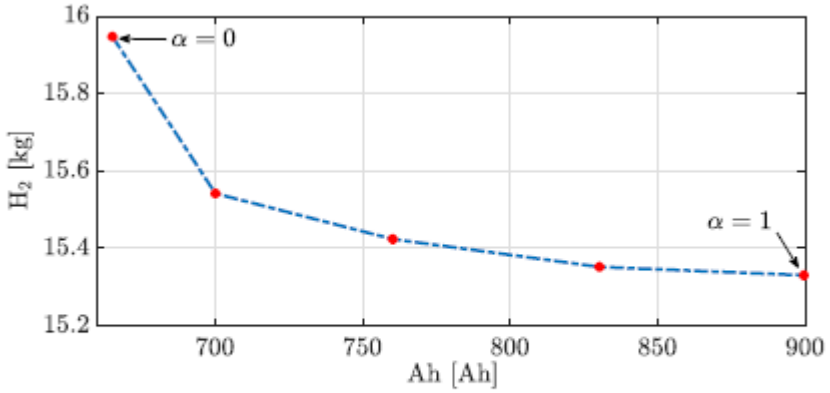

Figure 13: Pareto front.

Pareto front: In this work, the PMP results are evaluated for varying weighting factor α. The optimal results are analysed by drawing a pareto front of the total hydrogen consumption (in kg) caused in the fuel cell system against the total Ah throughput of the battery system, refer figure 13. The pareto front signifies that a significant increase in battery life can be achieved with a minimal increase in the hydrogen fuel consumption.

This relation holds, mainly because, hydrogen consumption is quadratic, refer (27) whereas the battery ageing is exponential in nature in relation to the power flow.

7 Conclusion

In this paper an energy management strategy for a hybrid vehicle using optimal control method Pontryagin's minimum principle has been implemented and analysed. By consideration of battery ageing minimisation along with the fuel cell consumption minimisation yielded an economical solution. The Pareto front confirms that the battery life can be prolonged significantly with a very little increase in fuel cell energy consumption. A minimal increase in fuel cell energy consumption of approx 1:4% resulted in almost 23% reduction in the total battery Ah throughput. Also, by consideration of the battery pack temperature dynamics along with the state of charge helped us to determine the actual severity factor s in the battery ageing mechanism. This absolute optimal energy consumption information serves as a benchmark for heuristic, online real-time control strategy design. The paper highlights that with increasing order of system dynamics and the corresponding increase in number of co-states, the differential evolutionary algorithm could be a very powerful and robust tool in determining the optimal initial co-states values.

Acknowledge

This work is funded by the BMVi under the National Innovation Programme Hydrogen and Fuel Cell Technology (NIP). The authors gratefully acknowledge the support by Siemens AG and NIP.

References

[1] Optimal energy management in a dual-storage fuel-cell hybrid vehicle using multidimensional dynamic programming. In: Journal of Power Sources 250 (2014), S. 359 – 371. http://dx.doi.org/https://doi.org/10.1016/j.jpowsour.2013.10.145. – DOI https://doi.org/10.1016/j.jpowsour.2013.10.145. – ISSN 0378–7753

[2] ALI, Ahmed M. ; SÖFFKER, Dirk: Towards Optimal Power Management of Hybrid Electric Vehicles in Real-Time: A Review on Methods, Challenges, and State-Of-The-Art Solutions. In: Energies 11 (2018), Nr. 3. http://dx.doi.org/10.3390/en11030476.– DOI 10.3390/en11030476. – ISSN 1996–1073

[3] BARRÉ, Anthony ; DEGUILHEM, Benjamin ; GROLLEAU, Sébastien ; GÉRARD, Mathias ; SUARD, Frédéric ; RIU, Delphine: A review on lithium-ion battery ageing mechanisms and estimations for automotive applications. In: Journal of Power Sources 241 (2013), 680 - 689. http://dx.doi.org/https://doi.org/10.1016/j.jpowsour.2013.05.040. – DOI https://doi.org/10.1016/j.jpowsour.2013.05.040. – ISSN 0378–7753

[4] BELLMAN, Richard: The theory of dynamic programming. In: Bull. Amer. Math. Soc. 60 (1954), 11, Nr. 6, 503–515. https://projecteuclid.org:443/euclid.bams/1183519147

[5] CASANELLAS, F.: Losses in PWM inverters using IGBTs. In: IEE Proceedings - Electric Power Applications 141 (1994), Sep., Nr. 5, S. 235–239. http://dx.doi.org/10.1049/ip-epa:19941349. – DOI 10.1049/ip–epa:19941349. – ISSN 1350–2352

[6] DAS, S. ; SUGANTHAN, P. N.: Differential Evolution: A Survey of the Stateof-the-Art. In: IEEE Transactions on Evolutionary Computation 15 (2011), Feb, Nr. 1, S. 4–31. http://dx.doi.org/10.1109/TEVC.2010.2059031. – DOI 10.1109/TEVC.2010.2059031. – ISSN 1089–778X

[7] FUENTES CABRERA, Juan C. ; COELLO COELLO, Carlos A.: Handling Constraints in Particle Swarm Optimization Using a Small Population Size. In: GEL-

BUKH, Alexander (Hrsg.) ; KURI MORALES, Ángel F. (Hrsg.): MICAI 2007: Advances in Artificial Intelligence. Berlin, Heidelberg : Springer Berlin Heidelberg, 2007, S. 41–51

[8] GUENTHER, S. ; HOFMANN, W.: Multi-objective tradeoffs in the design optimization of synchronous reluctance machines for electric vehicle application. In: 2015 IEEE International Electric Machines Drives Conference (IEMDC), 2015, S. 1715–1721

[9] JEONG, Jongryeol ; LEE, Daeheung ; KIM, Namwook ; ZHENG, Chunhua ; PARK, Yeong-Il ; CHA, Suk W.: Development of PMP-based power management strategy for a parallel hybrid electric bus. In: International Journal of Precision Engineering and Manufacturing 15 (2014), Feb, Nr. 2, 345–353. http://dx.doi.org/10.1007/s12541-014-0344-7. – DOI 10.1007/s12541–014– 0344–7. – ISSN 2005–4602

[10] KIM, Namwook ; CHA, Suk-Won ; PENG, Huei: Optimal Control of Hybrid Electric Vehicles Based on Pontryagin's Minimum Principle. In: IEEE Trans. Contr. Sys. Techn. 19 (2011), 09, S. 1279–1287. http://dx.doi.org/10.1109/TCST.2010.2061232. – DOI 10.1109/TCST.2010.2061232

[11] KIRK, D.E.: Optimal Control Theory: An Introduction. Dover Publications, 2004 (Dover Books on Electrical Engineering Series). https://books.google.de/books?id=fCh2SAtWIdwC. – ISBN 9780486434841

[12] LI, Huan ; RAVEY, Alexandre ; N'DIAYE, A ; DJERDIR, A: A Review of Energy Management Strategy for Fuel Cell Hybrid Electric Vehicle, 2017, S. 1–6

[13] LOPEZ-CRUZ, Irineo: Efficient evolutionary algorithms for optimal control. In: Wageningen University. Promotor: Prof. Dr. Ir. G. van Straten, co-promotor(en): Dr. Ir. G. van Willigenburg. - [S.l.] : [s.n.], 2002. - ISBN 9058086496 (2002), 01

[14] LORENZO, Serrao ; SIMONA, Onori ; YANN, Geuzennec ; GIORGIO, Rizzoni: A Novel Model-Based Algorithm for Battery Prognosis. In: In Proceedings of the Seventh IFAC Symposium on Fault Detection, Supervision and Safety of Technical Processes (SAFEPROCESS (2009), S. 923–928

[15] MESTHA, L. K. ; EVANS, P. D.: Analysis of on-state losses in PWM inverters. In: IEE Proceedings B - Electric Power Applications 136 (1989), July, Nr. 4, S. 189–195. http://dx.doi.org/10.1049/ip-b.1989.0025. – DOI 10.1049/ip–b.1989.0025. – ISSN 0143–7038

[16] MUSARDO, Cristian ; RIZZONI, Giorgio ; GUEZENNEC, Yann ; STACCIA, Benedetto: A-ECMS: An Adaptive Algorithm for Hybrid Electric Vehicle Energy

Management. In: European Journal of Control 11 (2005), Nr. 4, S. 509 – 524. http://dx.doi.org/https://doi.org/10.3166/ejc.11.509-524. – DOI https://doi.org/10.3166/ejc.11.509–524. – ISSN 0947–3580

[17] ONORI, Simona ; SERRAO, Lorenzo ; RIZZAONI, Giorgio: Hybrid Electric Vehicles

[18] ONORI, Simona ; SPAGNOL, Pierfrancesco ; MARANO, Vincenzo ; GUEZENNEC, Yann ; RIZZONI, Giorgio: A new life estimation method for lithium-ion batteries in plug-in hybrid electric vehicles applications. In: International Journal of Power Electronics 4 (2012), Nr. 3, S. 302–319

[19] PADOVANI, Thomas M. ; DEBERT, Maxime ; COLIN, Guillaume ; CHAMAILLARD, Yann: Optimal energy management strategy including battery health through thermal management for hybrid vehicles. In: IFAC Proceedings Volumes 46 (2013), Nr. 21, S. 384–389

[20] SIMONA, Onori ; LORENZO, Serrao ; RIZZONI, Giorgio: Hybrid Electric Vehicles Energy Management Strategies(EMS). In: Springer (2016), S. 3943–3948. ISBN 978–1–4471–6779–2

[21] SIMONA, Onori ; PIERFRANCESCO, Spagnol ; VINCENZO, Marano ; RIZZONI, Giorgio: A new life estimation method for lithium ion batteries in plug in hybrid electric vehicles applications. In: International Journal of Power Electronics 4 (2012), Nr. 7, S. 302–319

[22] TANG, L. ; RIZZONI, G. ; ONORI, S.: Energy Management Strategy for HEVs Including Battery Life Optimization. In: IEEE Transactions on Transportation Electrification 1 (2015), Oct, Nr. 3, S. 211–222. http://dx.doi.org/10.1109/TTE.2015.2471180. – DOI 10.1109/TTE.2015.2471180. – ISSN 2332–7782 [23] WANG, John ; LIU, Ping: Cycle-life model for graphite-LiFePO4 cells. In: Journal of Power Sources 196 (2011), Nr. 7, S. 3943– 3948. http://dx.doi.org/10.1016/j.powsour.2010.11.134. – DOI 10.1016/j.powsour.2010.11.134